Lithos 128-131 (2012) 73–83

Contents lists available at SciVerse ScienceDirect

Lithos

journal homepage: www.elsevier.com/locate/lithos

Recycling oceanic crust for continental crustal growth: Sr–Nd–Hf isotope evidence from granitoids in the western Junggar region, NW China

Gong-Jian Tang [a,b], Qiang Wang [a,*], Derek A. Wyman [c], Zheng-Xiang Li [d], Yi-Gang Xu [a], Zhen-Hua Zhao [a]

[a] State Key Laboratory of Isotope Geochemistry, Guangzhou Institute of Geochemistry, Chinese Academy of Sciences, Guangzhou 510640, China
[b] Graduate University of Chinese Academy of Sciences, Beijing 100049, China
[c] School of Geosciences, The University of Sydney, NSW 2006, Australia
[d] The Institute for Geoscience Research (TIGeR), Department of Applied Geology, Curtin University, GPO Box U1987, Perth, WA 6845, Australia

ARTICLE INFO

Article history:
Received 17 June 2011
Accepted 3 November 2011
Available online 11 November 2011

Keywords:
Crustal growth
Recycling oceanic crust
Adakites
Granites
Junggar
Central Asian Orogenic Belt

ABSTRACT

The juvenile component of accretionary orogenic belts has been declining since the Archean. As a result, there is often controversy regarding the contribution of oceanic basalts to Phanerozoic crustal growth, as in the case of the Central Asian Orogenic Belt (CAOB). Here we report on three groups of Late Carboniferous (316–305 Ma) granitoids in the western Junggar region of northern Xinjiang, NW China, which is part of the southwestern CAOB. They consist of adakites and I and A-type granites, and as a whole have the most depleted isotopic compositions ($\varepsilon_{Nd}(t) = +6 - +9$, $(^{87}Sr/^{86}Sr)_i = 0.7030–0.7045$, and $\varepsilon_{Hf}(t) = +12 - +16$) among the granitoids of the CAOB. These features are nearly identical to those of pre-Permian ophiolites in northern Xinjiang, and are clearly different from those of Carboniferous basalts in the western Junggar region. These relationships indicate that the granitoids were mainly derived from recycled oceanic crust by melting of subducted oceanic crust (e.g., adakites), and of the middle–lower crust of intra-oceanic arc that mainly consisted of oceanic crust (e.g., I and A-type granites). Based on evidence from the CAOB, we suggest that recycling of oceanic crust has made a significant contribution to continental crustal growth and evolution during the Phanerozoic.

1. Introduction

Oceanic crust recycling via the melting of subducted slabs is generally favored for the creation of trondhjemite, tonalite, and granodiorite batholiths that dominate the Archean cratonic nuclei (e.g., Martin et al., 2005; Mints et al., 2010). While the post-Archean formation of continental crust may have been episodic (Condie, 2000; Stein and Hofmann, 1994), evidence suggests that the proportion of juvenile crust generated in these episodes declined to 50% or less by the Phanerozoic (e.g., Belousova et al., 2010; Hawkesworth et al., 2010). Given the changes in the thermal state of the upper mantle since the Archean, and the increasingly transitory nature of conditions that favor slab melting (Peacock et al., 1994), the contribution of oceanic crust to Phanerozoic crustal growth episodes is often debated (e.g., Belousova et al., 2010; Collins et al., 2011; Condie, 2000; Hawkesworth et al., 2010).

The CAOB, for example, represents a site of major crustal growth in the Phanerozoic and is one of the largest accretionary orogenic belts in the world. Half of CAOB is considered to represent the addition of juvenile material (Jahn et al., 2000; Kröner et al., 2007; Sengör et al., 1993; Xiao et al., 2004, 2009). The most prominent feature of the CAOB is the vast expanse of granitoids and volcanic rocks characterized by positive $\varepsilon_{Nd}(t)$ values and young $T_{DM\text{-}Nd}$ model ages (Jahn et al., 2000; Wu et al., 2000). Genetic models for the development of the voluminous juvenile CAOB crust, however, remain highly controversial (Jahn, 2004; Windley et al., 2007, and references therein). Sengör et al. (1993) speculated that it was extracted directly from the mantle by subduction–accretion processes along a single and long-evolving magmatic arc from the early Cambrian (540 Ma) to the Permian (260 Ma). More recent accretionary growth models have interpreted the CAOB in terms of multiple, shorter-lived, subduction zones and features documented in the modern southwest Pacific, such as accretion of island arcs, oceanic islands, seamounts, accretionary wedges and microcontinents (e.g., Windley et al., 2007; Xiao et al., 2004, 2008). Alternatively, other researchers have argued that the juvenile crust of the CAOB, including the western Junggar region, was produced in a post-collisional setting by underplating of isotopically juvenile, mantle-derived melts (e.g., Chen and Arakawa, 2005; Jahn et al., 2000; Liu et al., 2005, 2009; Wu et al., 2000) or was related to a 280–275 Ma mantle plume (e.g., Zhang et al., 2010; Zhou et al., 2004, 2009).

In this work, we present new U–Pb and Hf analysis of zircons, coupled with whole rock Sr–Nd isotope and element analysis of Late Carboniferous granitoids from the Keramay plutons of the western

* Corresponding author.
E-mail address: wqiang@gig.ac.cn (Q. Wang).

0024-4937/$ – see front matter © 2011 Elsevier B.V. All rights reserved.
doi:10.1016/j.lithos.2011.11.003

Junggar region (Fig. 1). These granitoids have distinctive isotopic compositions characterized by positive whole rock $\varepsilon_{Nd}(t)$ and zircon $\varepsilon_{Hf}(t)$ and young T_{DM} and model ages that offer a unique opportunity for resolving controversies concerning continental crustal growth and recycling.

2. Geological background

The western Junggar region, surrounded by the Altay Orogen, Tianshan Orogen, Kazakhstan Plate and the Junggar Basin, is located in the southwestern part of the CAOB (Fig. 1). A conspicuous feature of the region is the abundance of Cambrian to late Carboniferous (ca. 523–332 Ma) ophiolitic mélanges (Xiao et al., 2008). No metamorphic basement or rocks older than the Cambrian ophiolites have been identified (Hu et al., 2000; Xiao et al., 2008; Zheng et al., 2007). Carboniferous and Devonian strata are widespread (An and Zhu, 2009). Basalts, andesitic basalts, andesites, and felsic tuff erupted mainly at ca. 350–330 Ma (Geng et al., 2011), although Late Carboniferous tholeiitic basalts in the Hatu area were formed at 315±4 Ma (Tang et al., submitted for publication).

Late Carboniferous granitoids are abundant in the central part of the study area, along with basalts and some mafic–felsic dikes (Fig. 1). The granitoids include (1) the Baogutu adakitic diorites and granodiorites (315–309 Ma), (2) the Keramay Group I-type granitoids (316–305 Ma), and (3) Miaoergou Group A-type granites (ca. 305 Ma) (Geng et al., 2009; Tang et al., 2010).

3. Analytical methods

3.1. Zircon U–Pb age analysis

Zircons were separated using conventional heavy liquid and magnetic separation techniques. Cathodoluminescence (CL) images were obtained for zircons prior to analysis, using a JEOL JXA-8100 Superprobe at the State Key Laboratory of Isotope Geochemistry (SKLIG), Guangzhou Institute of Geochemistry (GIG), Chinese Academy of Sciences (CAS), in order to characterize internal structures and choose potential target sites for U–Pb dating.

U–Pb isotope compositions of zircon grains were analyzed with an Agilent Q-ICPMS connected to a 193 nm excimer laser ablation system at the Institute of Geology and Geophysics, Chinese Academy of Sciences in Beijing, China (IGG-CAS). The GeoLas PLUS 193 nm excimer ArF laser ablation system is the upgraded product of GeoLas CQ made by Lambda Physik in Germany. Helium carrier gas transported the ablated sample materials from the laser-ablation cell via a mixing chamber to the ICPMS after mixing with Ar gas. Zircon 91500 was used as the standard and the standard silicate glass NIST 610 was used to optimize the machine, with a beam diameter of 30 μm. Raw count rates for ^{29}Si, ^{204}Pb, ^{206}Pb, ^{207}Pb, ^{208}Pb, ^{232}Th and ^{238}U were collected and U, Th and Pb concentrations were calibrated using ^{29}Si as the internal calibrant and NIST 610 as the reference material. $^{207}Pb/^{206}Pb$ and $^{206}Pb/^{238}U$ ratios were calculated using the GLITTER program (Jackson et al., 2004). Measured $^{207}Pb/^{206}Pb$, $^{206}Pb/^{238}U$ and $^{208}Pb/^{232}Th$ ratios in zircon 91500 were averaged over the course of the analytical session and used to calculate correction factors. These correction factors were then applied to each sample to correct for both instrumental mass bias and depth-dependent elemental and isotopic fractionation. Further detailed descriptions of the instrumentation and analytical procedure for the LA-ICP–MS zircon U–Pb technique can be found in Gao et al. (2002). The age calculations and plots were made using Isoplot (ver. 3.00) (Liu et al., 2010; Ludwig, 2003). The zircon U–Pb results are listed in Table 1.

3.2. Element and Nd–Sr isotope composition analysis

After crushing, fresher rock fractions were selected and subjected to ultrasonic cleaning in distilled water with <5% HNO_3 and distilled water, dried and handpicked to remove visible contamination, and then pulverized.

Major element oxides (wt.%) for whole rock powders were determined using a Varian Vista PRO ICP-AES at the SKLIG (GIG-CAS), and a wavelength X-ray fluorescence spectrometry with analytical errors

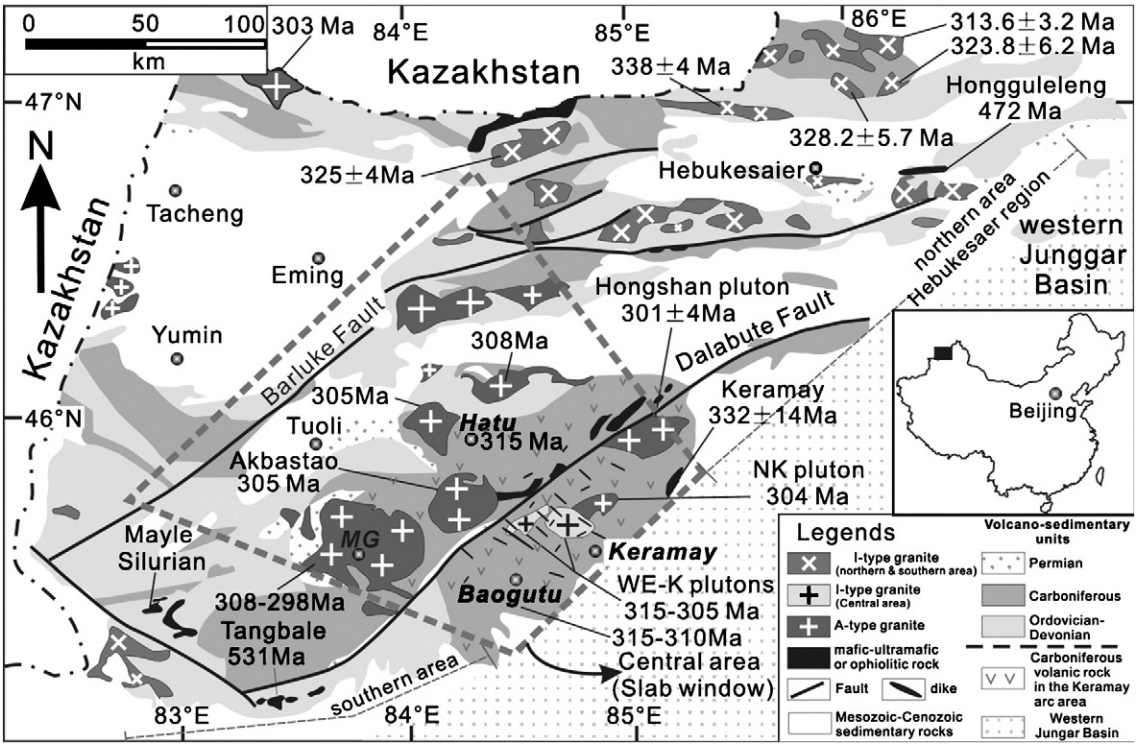

Fig. 1. Geological map of the western Junggar region (modified after Tang et al. (2010)). Small adakitic plutons (<6 km wide) in the Baogutu area are not shown (see Tang et al. (2010)). MG — Miaoergou granites. WE–K — western and eastern Keramay; NK — northern Keramay.

Table 1
LA-ICP–MS U–Pb isotopic analysis for zircons from Keramay plutons in the western Junggar region.

Analysis	Content (ppm)			Isotopic ratios						Isotopic ages (Ma)					
	Th	U	Th/U	$^{207}Pb/^{206}Pb$	±1σ	$^{207}Pb/^{235}U$	±1σ	$^{206}Pb/^{238}U$	±1σ	$^{207}Pb/^{206}Pb$	±1σ	$^{207}Pb/^{235}U$	±1σ	$^{206}Pb/^{238}U$	±1σ
06XJ120															
1	375	561	1.5	0.0527	0.0023	0.3623	0.0149	0.0499	0.0009	315	61	314	11	314	5
2	245	471	1.92	0.0613	0.0026	0.4167	0.0167	0.0493	0.0009	650	54	354	12	310	6
3	163	374	2.29	0.054	0.0031	0.367	0.0202	0.0493	0.001	371	86	317	15	310	6
4	195	395	2.03	0.06	0.0037	0.4115	0.0241	0.0498	0.001	602	90	350	17	313	6
5	175	310	1.78	0.0716	0.0037	0.4935	0.0235	0.05	0.0012	975	59	407	16	315	7
6	318	680	2.14	0.0531	0.0024	0.356	0.0152	0.0486	0.0009	333	63	309	11	306	6
7	355	811	2.29	0.0899	0.0019	0.622	0.0116	0.0502	0.0007	1422	17	491	7	316	4
8	271	549	2.03	0.0558	0.0026	0.3846	0.0168	0.05	0.001	444	62	330	12	315	6
9	242	238	0.98	0.0754	0.0058	0.5379	0.0378	0.0517	0.0019	1080	84	437	25	325	11
10	426	947	2.22	0.0726	0.0019	0.4982	0.0118	0.0498	0.0008	1003	25	410	8	313	5
11	207	524	2.53	0.0563	0.0025	0.3775	0.0157	0.0486	0.0009	465	60	325	12	306	5
12	364	719	1.97	0.0532	0.0034	0.3567	0.022	0.0487	0.0009	336	149	310	16	306	5
13	236	394	1.67	0.0542	0.0029	0.3678	0.0185	0.0492	0.001	379	77	318	14	310	6
14	266	580	2.18	0.0658	0.0024	0.4448	0.0148	0.049	0.0009	799	41	374	10	309	5
15	277	516	1.86	0.0669	0.0022	0.4638	0.0141	0.0503	0.0009	836	36	387	10	316	5
16	290	500	1.73	0.0767	0.003	0.5241	0.0187	0.0495	0.001	1114	41	428	12	312	6
17	506	847	1.67	0.06	0.0038	0.4112	0.0253	0.0497	0.0008	605	142	350	18	313	5
18	484	859	1.78	0.0556	0.0035	0.3732	0.0223	0.0487	0.0008	435	142	322	16	307	5
19	132	289	2.2	0.0761	0.0045	0.5248	0.029	0.05	0.0012	1097	73	428	19	315	7
20	209	419	2.01	0.0571	0.0029	0.3899	0.0189	0.0495	0.001	496	72	334	14	311	6
21	292	457	1.57	0.0573	0.0015	0.3927	0.0098	0.0497	0.0007	502	31	336	7	313	4
22	405	870	2.15	0.0558	0.0023	0.3752	0.0148	0.0488	0.0007	443	96	324	11	307	4
06XJ136															
1	124	160	0.77	0.0557	0.0043	0.3851	0.0278	0.0502	0.0016	439	104	331	20	316	10
2	239	240	1	0.0667	0.0081	0.4561	0.0529	0.0496	0.002	828	178	382	37	312	12
3	44	96	0.46	0.0576	0.0051	0.4536	0.0386	0.0572	0.0017	513	136	380	27	358	10
4	74	109	0.68	0.0573	0.0065	0.4522	0.049	0.0572	0.002	503	179	379	34	359	12
5	78	112	0.7	0.0543	0.0082	0.4187	0.0614	0.056	0.0019	382	330	355	44	351	12
6	93	143	0.65	0.0608	0.005	0.4391	0.0336	0.0524	0.0017	631	108	370	24	329	11
7	179	206	0.87	0.0526	0.0033	0.3586	0.0214	0.0495	0.0011	311	96	311	16	311	7
8	206	210	0.98	0.0541	0.0031	0.3799	0.0205	0.0509	0.0012	376	80	327	15	320	7
9	54	91	0.59	0.0691	0.0066	0.4747	0.0419	0.0499	0.002	901	117	394	29	314	12
10	121	176	0.68	0.0624	0.0049	0.4408	0.0319	0.0513	0.0018	687	96	371	22	322	11
11	174	238	0.73	0.0607	0.0035	0.4286	0.0229	0.0512	0.0013	630	71	362	16	322	8
12	144	186	0.77	0.0562	0.0032	0.3857	0.0204	0.0498	0.0012	461	75	331	15	313	7
13	218	234	0.93	0.0684	0.0059	0.4709	0.0368	0.05	0.0019	880	99	392	25	314	12
14	82	114	0.72	0.0629	0.0046	0.4293	0.0296	0.0496	0.0013	704	101	363	21	312	8
15	127	163	0.78	0.0533	0.0026	0.3766	0.0171	0.0513	0.001	340	68	325	13	323	6
16	65	209	0.31	0.0543	0.0036	0.3585	0.0227	0.0479	0.0008	384	152	311	17	301	5
17	86	163	0.53	0.0558	0.0033	0.3788	0.021	0.0493	0.0012	445	81	326	15	310	7
18	124	202	0.61	0.056	0.0025	0.4403	0.0179	0.0571	0.0011	452	56	370	13	358	7
06XJ182															
1	97	118	0.82	0.0739	0.0061	0.5635	0.0452	0.0553	0.0014	1038	122	454	29	347	8
2	84	118	0.71	0.0648	0.0054	0.4615	0.0357	0.0517	0.0018	768	104	385	25	325	11
3	84	107	0.79	0.0671	0.0063	0.479	0.042	0.0518	0.0019	841	121	397	29	325	12
4	356	324	1.1	0.0527	0.002	0.3563	0.0127	0.0491	0.0009	314	49	309	9	309	5
5	273	271	1.01	0.0578	0.0035	0.4013	0.0226	0.0504	0.0013	522	79	343	16	317	8
6	158	139	1.14	0.0634	0.0064	0.4427	0.0432	0.0507	0.0015	721	159	372	30	319	9
7	612	931	0.66	0.0665	0.0015	0.5541	0.0111	0.0605	0.0009	822	20	448	7	378	5
8	121	131	0.93	0.0634	0.0041	0.4353	0.0258	0.0498	0.0014	721	79	367	18	314	9
9	171	165	1.04	0.0675	0.0036	0.5291	0.0266	0.0569	0.0012	852	68	431	18	357	8
10	161	165	0.97	0.0718	0.0043	0.5641	0.0313	0.057	0.0016	979	68	454	20	358	10
11	271	220	1.23	0.0576	0.0025	0.3903	0.0162	0.0491	0.0009	516	58	335	12	309	6
12	85	112	0.75	0.0695	0.0076	0.4705	0.049	0.0491	0.0018	914	156	391	34	309	11
13	169	153	1.1	0.0709	0.0078	0.4977	0.0531	0.051	0.0016	954	168	410	36	320	10
14	198	183	1.08	0.0606	0.0041	0.4235	0.0263	0.0507	0.0015	626	84	359	19	319	9
15	246	228	1.08	0.0586	0.0044	0.4137	0.03	0.0512	0.0011	553	120	352	22	322	7
16	265	279	0.95	0.0612	0.0057	0.4674	0.0419	0.0554	0.0012	647	206	389	29	347	7
17	135	146	0.92	0.0665	0.0056	0.5224	0.0417	0.057	0.0018	822	114	427	28	357	11
18	132	150	0.88	0.0688	0.0131	0.4799	0.0899	0.0506	0.0017	892	422	398	62	318	10
19	183	277	0.66	0.0703	0.0039	0.5412	0.0276	0.0558	0.0015	937	62	439	18	350	9
20	222	252	0.88	0.0611	0.0041	0.4286	0.0268	0.0509	0.0015	641	84	362	19	320	9
21	219	231	0.95	0.0642	0.0047	0.4573	0.0312	0.0517	0.0015	747	94	382	22	325	9
22	123	155	0.79	0.055	0.0047	0.3739	0.0307	0.0493	0.0014	413	131	323	23	310	9

better than 2%. FeO contents of some samples were analyzed by conventional methods at the HIGMR. Details of the analytical procedures at the SKLIG were described by Li et al. (2002). Trace elements, including the rare earth element (REE), were analyzed using a Perkin-Elmer ELAN 6000 inductively-coupled plasma source mass spectrometer (ICP-MS) at the SKLIG, following procedures described

by Li et al. (2002). Analytical precision for most elements is better than 3%, and the trace element contents for International Reference Materials measured during this study are listed Appendix-1.

Sr and Nd isotopic compositions of selected samples were determined using a Micromass Isoprobe multi-collector mass spectrometer (MC-ICPMS) at the SKLIG (GIG-CAS). Analytical procedures are similar to that described in Li et al. (2006). The $^{87}Sr/^{86}Sr$ ratio of the NBS987 standard and $^{143}Nd/^{144}Nd$ ratio of the Shin Etsu JNdi-1 standard measured were 0.710288 ± 28 (2σm) and 0.512109 ± 12 (2σm), respectively. All measured $^{143}Nd/^{144}Nd$ and $^{86}Sr/^{88}Sr$ ratios are fractionation corrected to $^{146}Nd/^{144}Nd = 0.7219$ and $^{86}Sr/^{88}Sr = 0.1194$, respectively. The results are listed in Table 2.

3.3. Zircon Hf isotope analysis

In situ zircon Hf isotopic analysis were conducted using a Neptune MC–ICPMS, equipped with a 193-nm laser, at IGG-CAS. During analysis, spot sizes of 32 and 63 mu, with a laser repetition rate of 10 Hz at 100 mJ, were used and raw count rates for ^{172}Yb, ^{173}Yb, ^{175}Lu, $^{176}(Hf+Yb+Lu)$, ^{177}Hf, ^{178}Hf, ^{179}Hf, ^{180}Hf and ^{182}W were collected. During laser ablation analysis the isobaric interference of ^{176}Lu on ^{176}Hf is negligible due to the extremely low $^{176}Lu/^{177}Hf$ in zircon (normally <0.002). However, the interference of ^{176}Yb on ^{176}Hf must be carefully corrected since the contribution of ^{176}Yb to ^{176}Hf could profoundly affect the accuracy of the measured $^{176}Hf/^{177}Hf$ ratio. In this project, the mean $^{173}Yb/$

Table 2
Major (wt.%) and trace (ppm) element and Sr–Nd isotopic compositions of the Keramay plutons.

Sample	06XJ120	06XJ121.1	06XJ127	06XJ131	06XJ136	06XJ170	06XJ174	06XJ179	06XJ182
Location	NK	NK	WK	WK	EK	EK	EK	EK	EK
SiO_2	73.83	74.06	69.82	75.12	54.78	60.36	70.03	66.77	64.10
TiO_2	0.21	0.21	0.36	0.17	0.99	0.88	0.48	0.54	0.74
Al_2O_3	13.58	13.56	14.81	13.51	17.35	16.88	14.84	15.47	15.43
FeO^{Total}	1.34	1.23	2.35	0.75	7.46	5.57	2.73	3.45	4.62
MnO	0.03	0.03	0.07	0.02	0.12	0.09	0.04	0.05	0.08
MgO	0.32	0.34	1.29	0.34	4.35	3.62	1.37	1.77	2.46
CaO	0.97	1.04	2.61	1.26	7.87	5.20	2.43	3.71	4.11
Na_2O	4.04	4.01	4.40	3.77	3.54	3.63	3.46	4.12	4.05
K_2O	4.72	4.67	2.35	4.08	1.20	1.90	3.24	1.52	2.46
P_2O_5	0.03	0.03	0.08	0.03	0.16	0.12	0.07	0.09	0.11
LOI	0.27	0.16	1.12	0.34	0.89	0.73	0.56	1.71	0.86
Total	99.48	99.48	99.53	99.47	99.56	99.60	99.55	99.57	99.53
$Mg^{\#}$	29.9	32.9	49.5	44.3	50.9	53.6	47.2	47.7	48.6
Sc	4.03	4.26	6.16	2.23	22.2	15.5	6.98	8.70	12.3
V	10.7	10.5	43.7	10.9	201	134	54.7	88.1	109
Cr	1.24	1.52	25.1	0.9	94.6	83.8	17.3	25.0	44.3
Co	46.4	34.7	27.1	60.2	48.7	43.8	29.4	53.8	33.7
Ni	3.13	3.03	19.1	3.99	43.4	52.5	10.7	17.9	25.9
Ga	19.8	19.1	15.3	12.9	19.4	17.7	13.6	17.0	17.3
Cs	2.95	3.00	0.851	2.56	0.819	1.35	1.52	1.26	1.22
Rb	112	101	41.9	123	20.1	39.5	71.8	52.9	50.9
Ba	344	364	657	830	351	532	687	305	603
Th	11.1	8.34	6.04	18.3	2.17	3.08	7.70	5.57	4.23
U	1.42	1.36	0.958	2.55	0.515	0.57	1.45	1.39	1.04
Pb	14.3	14.1	4.04	16.2	5.02	5.78	5.47	4.44	5.69
Nb	7.48	6.55	3.42	3.74	4.11	4.22	3.87	4.03	4.82
Ta	0.919	0.637	0.419	0.822	0.366	0.398	0.495	0.502	0.462
Sr	79.4	88.7	424	190	502	453	242	397	356
Y	41.6	29.9	15.7	8.84	22.4	17.5	13.6	14.9	18.6
Zr	159	167	104	106	97.4	104	124	112	118
Hf	6.24	6.31	3.44	3.98	3.27	3.21	3.89	3.38	3.62
La	31.6	31.0	12.8	19.1	13.1	12.0	12.8	15.4	13.8
Ce	70.9	72.6	29.1	35.6	33.1	27.8	27.2	33.8	31.0
Pr	9.21	8.73	3.73	3.79	4.64	3.76	3.42	4.22	4.04
Nd	35.6	32.8	15.0	12.5	19.8	16.0	13.2	16.0	16.3
Sm	7.37	6.29	3.11	1.97	4.43	3.55	2.64	3.08	3.43
Eu	0.474	0.532	0.890	0.405	1.27	1.02	0.678	0.75	0.905
Gd	6.83	5.58	2.93	1.75	4.37	3.36	2.53	2.76	3.33
Tb	1.22	0.947	0.473	0.255	0.711	0.543	0.409	0.432	0.553
Dy	7.49	5.69	2.83	1.46	4.10	3.24	2.37	2.49	3.28
Ho	1.59	1.19	0.572	0.308	0.854	0.639	0.482	0.512	0.685
Er	4.68	3.47	1.64	0.917	2.41	1.82	1.41	1.46	1.96
Tm	0.729	0.518	0.239	0.153	0.345	0.266	0.212	0.217	0.301
Yb	4.94	3.46	1.59	1.12	2.27	1.69	1.45	1.50	1.00
Lu	0.766	0.546	0.252	0.194	0.345	0.257	0.230	0.237	0.305
$^{87}Sr/^{86}Sr$	0.721880	0.718282	0.704975	0.712751	0.704211	0.704118	0.704177	0.705460	0.705426
2σ	0.000013	0.000011	0.000014	0.000016	0.000013	0.000013	0.000011	0.000020	0.000018
$^{87}Rb/^{86}Sr$	3.9729	3.2129	0.2791	1.8207	0.1131	0.2458	0.8360	0.3754	0.4033
$^{143}Nd/^{144}Nd$	0.512929	0.512884	0.512898	0.512819	0.512900	0.512917	0.512852	0.512889	0.512922
2σ	0.000006	0.000008	0.000006	0.000006	0.000006	0.000007	0.000010	0.000009	0.000007
$^{147}Sm/^{144}Nd$	0.1258	0.1167	0.1266	0.0964	0.1362	0.1350	0.1218	0.1168	0.1285
$(^{87}Sr/^{86}Sr)_i$	0.70464	0.70434	0.70376	0.70485	0.70372	0.70305	0.70055	0.70383	0.70368
$(^{143}Nd/^{144}Nd)_i$	0.51268	0.51265	0.51265	0.51263	0.51263	0.51265	0.51261	0.51266	0.51267
$\varepsilon_{Nd}(t)$	8.4	7.9	7.8	7.4	7.5	7.9	7.1	8.0	8.2
T_{DM}	386	421	444	433	495	454	497	413	411
$f_{Sm/Nd}$	−0.36	−0.41	−0.36	−0.51	−0.31	−0.31	−0.38	−0.41	−0.35

^{171}Yb ratio of the individual spots was used to calculate the fractionation coefficient (βYb), and then to calculate the contribution of ^{176}Yb to ^{176}Hf. During analysis, an isotopic ratio of ^{176}Yb/^{172}Yb = 0.5887 was applied. The detailed analytical technique is described in Wu et al. (2006). During the analytical period, the ^{176}Hf/^{177}Hf and ^{176}Lu/^{177}Hf ratios of the standard zircon (91500) were 0.282294 ± 15 (2σ, n = 20) and 0.00031. Zircon Lu–Hf isotopic data are listed in Table 3.

4. Results

The U–Pb data are summarized in Fig. 2. Zircon grains from NK (sample 06XJ120), WK (sample 06XJ136) and EK (sample 06XJ182) plutons exhibit concentric compositional zoning and high Th/U ratios (0.31–1.02), suggesting a magmatic origin. Twenty-two, fourteen and fifteen analytical spots of zircons from samples 06XJ120, 06XJ136 and 06XJ183 yield weighted mean ^{206}Pb/^{238}U age of 304 ± 3 Ma, 314 ± 3 Ma and 316 ± 3 Ma, respectively. Based on these results and previously published zircon U–Pb age data (Geng et al., 2009; Han et al., 2006), we suggest that the WK and EK plutons were generated at 316–305 Ma, and the NK pluton formed at ~304 Ma, contemporaneously with the ~305 Ma Miaoergou granites.

The Miaoergou Group (i.e., Miaoergou and NK) consists of high-silica alkali-feldspar granites (Fig. 3a; Table 2) (Chen and Arakawa, 2005; Chen and Jahn, 2004; Geng et al., 2009). They display either light rare earth element (REEs) enriched or unfractionated REE patterns, all with strongly negative Eu, Ba and Sr anomalies (Fig. 6 of

Table 3
Lu–Hf isotopic compositions of zircons from the Keramay plutons.

Sample	^{176}Yb/^{177}Hf	^{176}Lu/^{177}Hf	^{176}Hf/^{177}Hf	2σ	$(^{176}Hf/^{177}Hf)_i$	$\varepsilon_{Hf}(t)$	T_{DM}(Ma)	$f_{Lu/Hf}$
06XJ120 01	0.097689	0.002627	0.283036	0.000030	0.283021	15.5	320	−0.92
06XJ120 02	0.066996	0.001844	0.283006	0.000031	0.282995	14.6	357	−0.94
06XJ120 03	0.065087	0.001834	0.283042	0.000029	0.283032	15.9	304	−0.94
06XJ120 04	0.085450	0.002658	0.283040	0.000025	0.283024	15.6	314	−0.92
06XJ120 05	0.066366	0.001936	0.282961	0.000029	0.282950	13.0	423	−0.94
06XJ120 06	0.110526	0.003089	0.283040	0.000033	0.283022	15.5	318	−0.91
06XJ120 07	0.087908	0.002646	0.282967	0.000026	0.282952	13.1	423	−0.92
06XJ120 09	0.089402	0.002471	0.283037	0.000033	0.283022	15.6	318	−0.93
06XJ120 10	0.095945	0.002830	0.283039	0.000024	0.283023	15.6	317	−0.91
06XJ120 11	0.063456	0.001887	0.283012	0.000028	0.283001	14.8	349	−0.94
06XJ120 12	0.102793	0.003319	0.282978	0.000037	0.282959	13.3	414	−0.90
06XJ120 13	0.084766	0.002461	0.282964	0.000030	0.282950	13.0	425	−0.93
06XJ120 14	0.090011	0.002578	0.282983	0.000030	0.282968	13.6	398	−0.92
06XJ120 15	0.086534	0.002616	0.283051	0.000024	0.283036	16.0	298	−0.92
06XJ120 16	0.066331	0.002071	0.283035	0.000026	0.283023	15.6	317	−0.94
06XJ120 17	0.103883	0.003040	0.283039	0.000036	0.283021	15.5	320	−0.91
06XJ120 18	0.088970	0.002727	0.282949	0.000029	0.282933	12.4	450	−0.92
06XJ120 19	0.051365	0.001620	0.283007	0.000036	0.282998	14.7	352	−0.95
06XJ120 20	0.077120	0.002473	0.283008	0.000031	0.282993	14.5	361	−0.93
06XJ120 21	0.109314	0.003005	0.283010	0.000022	0.282993	14.5	362	−0.91
06XJ120 22	0.094133	0.002840	0.283055	0.000014	0.283039	16.1	293	−0.91
06XJ136 01	0.077818	0.002339	0.283028	0.000060	0.283015	15.5	329	−0.93
06XJ136 02	0.118484	0.003467	0.282967	0.000069	0.282947	13.1	433	−0.90
06XJ136 03	0.023953	0.000789	0.283028	0.000031	0.283024	16.8	315	−0.98
06XJ136 04	0.052863	0.001826	0.283035	0.000030	0.283025	16.8	314	−0.94
06XJ136 05	0.069353	0.002287	0.283028	0.000051	0.283015	16.3	329	−0.93
06XJ136 06	0.063794	0.002113	0.282951	0.000044	0.282939	12.8	440	−0.94
06XJ136 07	0.091643	0.002841	0.283018	0.000047	0.283002	15.0	348	−0.91
06XJ136 08	0.081629	0.002551	0.283004	0.000020	0.282990	14.6	366	−0.92
06XJ136 09	0.029035	0.000958	0.283013	0.000043	0.283008	15.2	338	−0.97
06XJ136 10	0.051130	0.001742	0.283041	0.000055	0.283031	16.1	305	−0.95
06XJ136 11	0.079016	0.002329	0.282980	0.000032	0.282967	13.8	399	−0.93
06XJ136 12	0.107781	0.003270	0.283018	0.000029	0.282999	14.9	353	−0.90
06XJ136 13	0.058272	0.001731	0.283034	0.000026	0.283024	15.8	316	−0.95
06XJ136 14	0.083596	0.002348	0.283030	0.000027	0.283016	15.5	327	−0.93
06XJ136 15	0.032608	0.000950	0.283011	0.000028	0.283005	15.2	342	−0.97
06XJ136 16	0.030015	0.001002	0.282980	0.000039	0.282974	14.0	386	−0.97
06XJ136 17	0.030626	0.000988	0.282991	0.000024	0.282985	15.4	370	−0.97
06XJ136 18	0.040176	0.001261	0.283004	0.000031	0.282996	16.8	354	−0.96
06XJ182 01	0.093625	0.002766	0.283012	0.000028	0.282996	15.5	357	−0.92
06XJ182 02	0.072888	0.002064	0.283020	0.000040	0.283008	15.3	338	−0.94
06XJ182 03	0.075718	0.002222	0.282963	0.000037	0.282950	13.2	424	−0.93
06XJ182 04	0.165599	0.004889	0.283040	0.000038	0.283012	15.4	335	−0.85
06XJ182 05	0.167137	0.004581	0.283048	0.000037	0.283021	15.8	320	−0.86
06XJ182 06	0.088628	0.002659	0.283030	0.000054	0.283014	15.5	329	−0.92
06XJ182 07	0.154937	0.004191	0.283020	0.000031	0.282996	16.0	359	−0.87
06XJ182 08	0.098894	0.002722	0.283027	0.000040	0.283011	15.4	334	−0.92
06XJ182 10	0.081412	0.002273	0.283027	0.000037	0.283013	16.4	331	−0.93
06XJ182 11	0.128430	0.003501	0.283013	0.000034	0.282993	14.7	363	−0.89
06XJ182 12	0.086041	0.002573	0.282960	0.000041	0.282945	13.1	433	−0.92
06XJ182 13	0.092880	0.002696	0.282998	0.000055	0.282983	14.4	377	−0.92
06XJ182 14	0.128505	0.003728	0.282971	0.000056	0.282950	13.2	429	−0.89
06XJ182 15	0.130517	0.003551	0.283014	0.000034	0.282993	14.8	362	−0.89
06XJ182 16	0.099614	0.002866	0.282951	0.000062	0.282935	13.5	449	−0.91
06XJ182 17	0.131183	0.003957	0.282919	0.000114	0.282896	11.3	513	−0.88
06XJ182 18	0.126402	0.003721	0.283042	0.000035	0.283020	15.7	321	−0.89
06XJ182 19	0.127125	0.003598	0.283015	0.000037	0.282994	14.8	361	−0.89
06XJ182 20	0.108181	0.003198	0.282958	0.000055	0.282939	12.9	443	−0.90

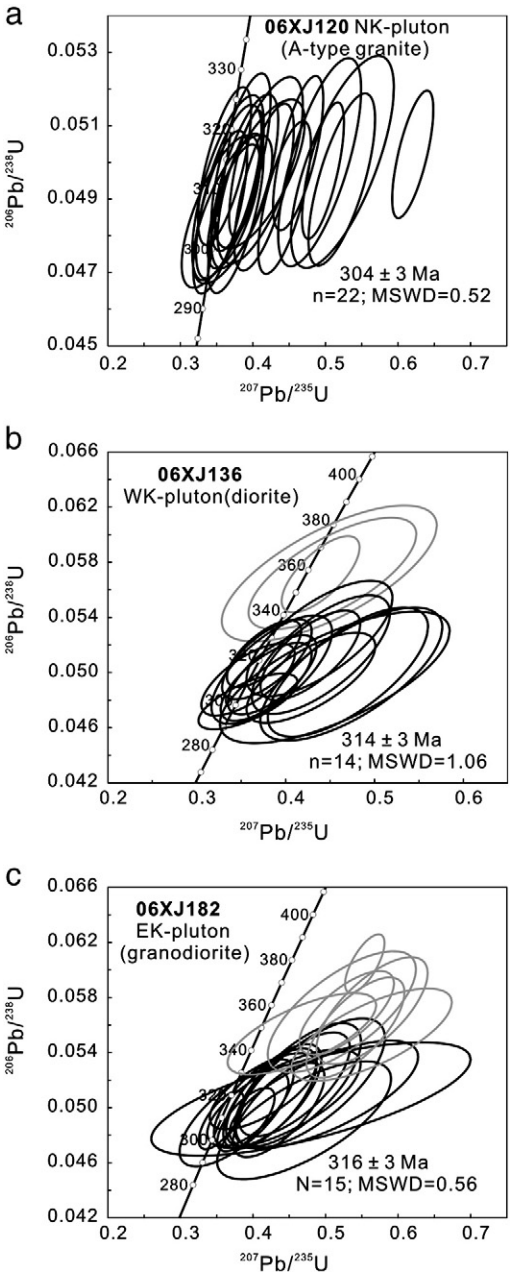

Fig. 2. LA-ICP–MS zircon U–Pb Concordia plots for the Keramay plutons in the western Junggar region.

Tang et al. (2010)) and high 10,000× Ga/Al and FeO/MgO ratios and Zr and Zr + Ce + Nb + Y contents, which are distinct from highly fractionated granites but similar to typical A-type granites (Fig. 3b–d) (Eby, 1990, 1992; Kemp and Hawkesworth, 2003; Whalen et al., 1987). Moreover, A-type granites generally have high zircon saturation temperatures relative to highly fractionated I-type granites (King et al., 1997). Calculated zircon saturation temperatures (Tzr) of the Miaoergou group granites range from 826 to 976 °C. Their average value of 931 °C (Tang, 2011; Tang et al., 2010), is distinctly higher than the 781 °C average of the highly fractionated I-type granitoids but consistent with the 927 °C average of typical A-type granites (Whalen et al., 1987).

The EK–WK diorites and granodiorites have variable SiO_2 (53.36–75.12 wt.%), MgO (0.34–5.81 wt.%) and Ni (3.99–69.2 ppm) contents (Table 2) (Chen and Arakawa, 2005; Chen and Jahn, 2004; Tang, 2011). They are medium-K calc-alkaline, and have moderate Sr (290–508 ppm) and Yb (0.62–1.91 ppm) concentrations, Sr/Y (17–26) and La_N/Yb_N (2.1–17) ratios (Fig. 3e–f), and enriched light REEs relative to heavy REEs and weakly negative Eu anomalies (Fig. 6 of Tang et al. (2010); Table 2) (Chen and Arakawa, 2005; Tang, 2011), similar to typical I-type granites (Chappell and White, 1992; Konopelko et al., 2007). The Baogutu adakites are characterized by high Sr concentrations (452–684 ppm) and Sr/Y ratios (34–52), strongly fractionated REE patterns and no Eu anomalies (Fig. 6 of Tang et al. (2010)). They plot in the field of typical "adakites", and display much lower Y and Yb contents but clearly higher Sr/Y and $(La/Yb)_N$ ratios than the Keramay group I type granitoids (Fig. 3e–f). Some of the intrusions are geochemically similar to high-Mg andesites (Tang et al., 2010). On discrimination diagrams for low-SiO_2-adakites (LSA) and high-SiO_2-adakites (HSA) (Fig. 9 of the Tang et al. (2010)), the Baogutu adakites mainly plot in the field of HAS. The Baogutu adakites and Keramay I-type granites are characterized by relatively high $Mg^{\#}$ values compared to the Miaoergou A-type granites (Fig. 3a).

All of the granites are characterized by depleted Nd-Sr isotope compositions ($\varepsilon_{Nd}(t) = +6$–$+9$, $(^{87}Sr/^{86}Sr)_i = 0.7030$–$0.7045$ and distinctly juvenile Nd model ages ($T_{DM\text{-}Nd}$) of 320–640 Ma) (Fig. 4, Table 2). Compared with the Miaoergou Group A-type granites and the Keramay I-type granites, the Baogutu adakities originating from subducted basaltic oceanic crust and minor sediments tend to have slightly lower $\varepsilon_{Nd}(t)$ and older $T_{DM\text{-}Nd}$ values (Fig. 4) (Tang et al., 2010). However, all of the intrusive rocks have higher $\varepsilon_{Nd}(t)$ values and lower $(^{87}Sr/^{86}Sr)_i$ values than those of the coeval Hatu tholeiites ($\varepsilon_{Nd}(t) = +5.3$–$+6.0$, $(^{87}Sr/^{86}Sr)_i = 0.7047$–$0.7067$) and Early Carboniferous mafic volcanic rocks ($\varepsilon_{Nd}(t) = +3.9$–$+6.8$, $(^{87}Sr/^{86}Sr)_i = 0.7031$–$0.7055$) (Fig. 4; Table 2) of the western Junggar area.

The Miaoergou Group A-type granites and Keramay I-type have highly depleted zircon $^{176}Hf/^{177}Hf$ isotopic compositions with $\varepsilon_{Hf}(t)$ values of +12 to +16 and young zircon Hf model ages (450–300 Ma) (Fig. 4f; Table 3). The Baogutu adaktes also have depleted whole rock Hf isotope compositions, with $\varepsilon_{Hf}(t)$ values of $\varepsilon_{Hf}(t)$ (+12.5 to 15.7) (Tang et al., 2010).

5. Discussion

5.1. Magmatic source

As a whole, the three granitoid groups have the most depleted isotopic compositions ($\varepsilon_{Nd}(t) = +6$–$+9$, $(^{87}Sr/^{86}Sr)_i = 0.7030$–$0.7045$, and $\varepsilon_{Hf}(t) = +12$–$+16$) among the granitoids of the CAOB (e.g., Jahn et al., 2000). Their remarkably depleted $(^{87}Sr/^{86}Sr)_i$, $\varepsilon_{Nd}(t)$ and $\varepsilon_{Hf}(t)$ isotopic compositions distinguish them from Neoproterozoic basement in the Tianshan and Altay areas, which have distinctly negative $\varepsilon_{Nd}(t)$ and high $(^{87}Sr/^{86}Sr)_i$ (>0.706) values (Hu et al., 2000) (Fig. 4). The fact that the young whole rock Nd and zircon Hf model ages of the Keramay area intrusions (Fig. 4; Table 2) differ markedly from any plausible ancient basement is consistent with the observation that no ancient continental crust has been recognized in the western Junggar region (Hu et al., 2000).

The isotopic compositions of Carboniferous mantle sources in the western Junggar region are represented by normal Early Carboniferous arc-type basalts-basaltic andesites (Geng et al., 2011) and Late Carboniferous Hatu tholeiitic basalts (Tang et al., submitted for publication). These mantle sources also cannot account for the extremely depleted Sr-Nd-Hf isotopic compositions of the Keramay granitoids based on the following evidence: (1) the granitoids have much higher $\varepsilon_{Nd}(t)$ (+6 to +9) values than those of the Early Carboniferous basalts and andesites ($\varepsilon_{Nd}(t) = +3.9$ to $+6.8$; Fig. 4; Table 2); (2) the intrusive rocks generally have $(^{87}Sr/^{86}Sr)_i$ values <0.7045 whereas most samples of Carboniferous basalts and andesites exhibit higher $(^{87}Sr/^{86}Sr)_i$ values (>0.7045) (Fig. 4), and (3) most importantly, the intrusions show much more depleted Sr–Nd–Hf isotope compositions than those of the contemporary Hatu basalts (Fig. 4). Therefore, the Miaoergou group A-type granites could not be generated by fractional

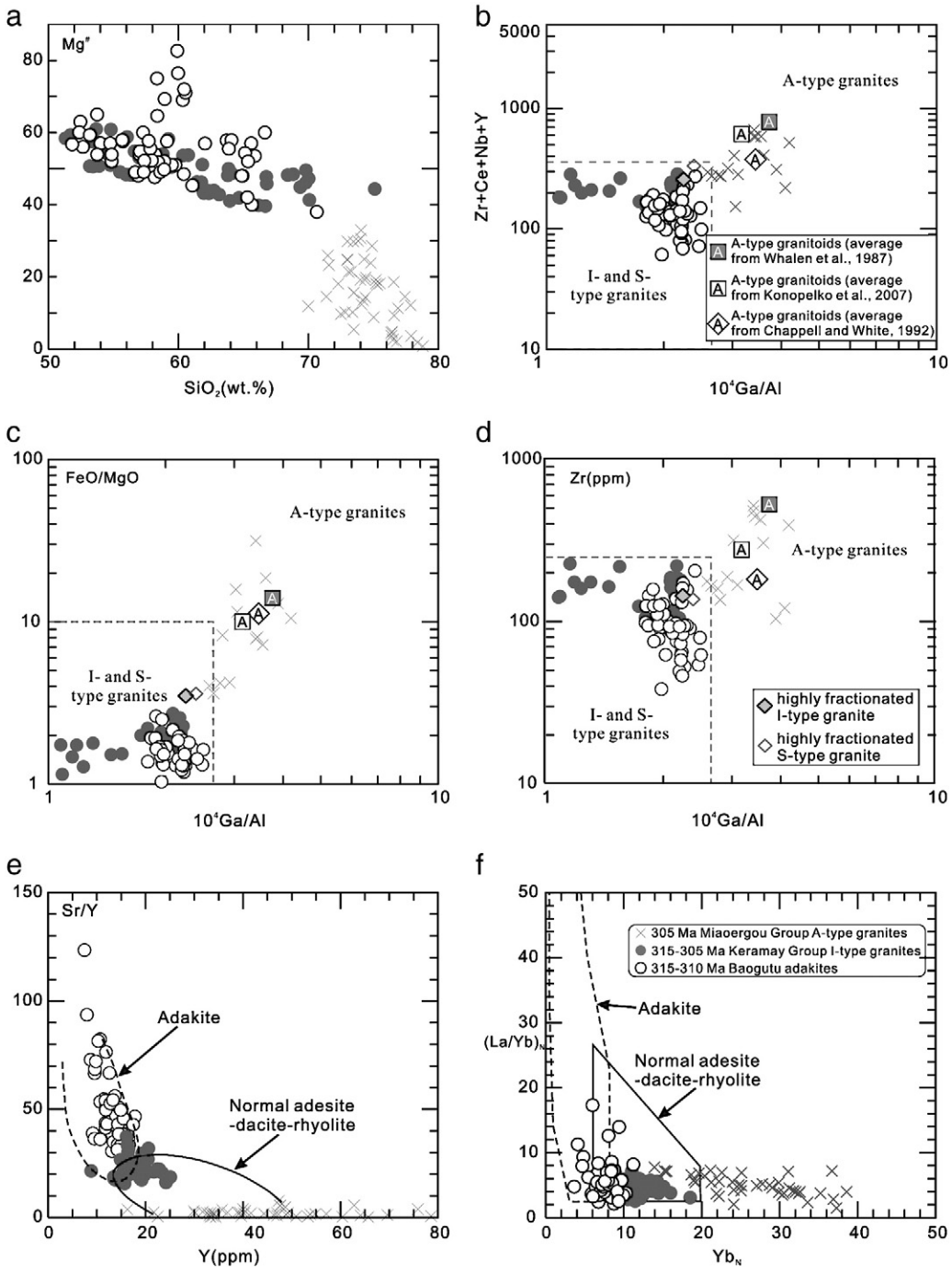

Fig. 3. Essential diagnostic geochemical discrimination diagrams for three group granitoids. (a) SiO_2 versus $Mg^{\#}$; (b–d) A-type granite discrimination diagrams (Whalen et al., 1987); (e) Sr/Y versus Y (Defant and Drummond, 1993); (f) La_N/Yb_N versus Yb_N (Drummond and Defant, 1990). The granitoid data are from Chen and Arakawa (2005), Geng et al.(2009, 2011), Shen et al. (2009), Tang et al.(2010), Tang (2011) and this study.

crystallization of mantle-derived arc basalt melts. In addition, given that Carboniferous western Junggar arc crust likely consisted of Early Carboniferous volcanic rocks (basalts and basaltic andesites) with relatively low εNd(t) (+3.9–+6.8) values (Geng et al., 2009), the high εNd(t) (+6–+9) of the A-type granites could not have been generated by arc crust melting (Kemp and Hawkesworth, 2003).

The depleted Sr–Nd–Hf isotope compositions of the western Junggar granitoids are consistent with a recycled oceanic crustal component, such as the mainly Cambrian-Carboniferous North Xinjiang ophiolites. Basalts from the ophiolites surrounding the Junggar Basin have high $\varepsilon_{Nd}(t)$ values of ~+8 to +11, as do associated plagiogranites (+7.5 to +9.5) (Fig. 4; Table 4). On a $(^{87}Sr/^{86}Sr)_i$–$\varepsilon_{Nd}(t)$ diagram (Fig. 4c), the field of the three granitoid group samples partially overlies that of the North Xinjiang ophiolites, and on a T (age)–$\varepsilon_{Nd}(t)$ diagram (Fig. 4d), they plot in the evolution field of these ophiolites. The plagiogranite samples from the ophiolites plot in the field of the Keramay granitoids (Fig. 4). Furthermore, the 523 Ma to 344 Ma emplacement age range, and mainly Late Devonian to Carboniferous Nd model ages, of the north Xinjiang ophiolites is comparable to the span of Nd and Hf model ages from the Karamey granitoids (Fig. 4). The Keramay area intrusions also plot in the field of the mid-ocean-ridge basalts on a $\varepsilon_{Nd}(t)$–$\varepsilon_{Hf}(t)$ diagram (Fig. 4). The isotopic data therefore provide powerful evidence for the oceanic crust components to be the dominant source for all three Keramay granitoid types.

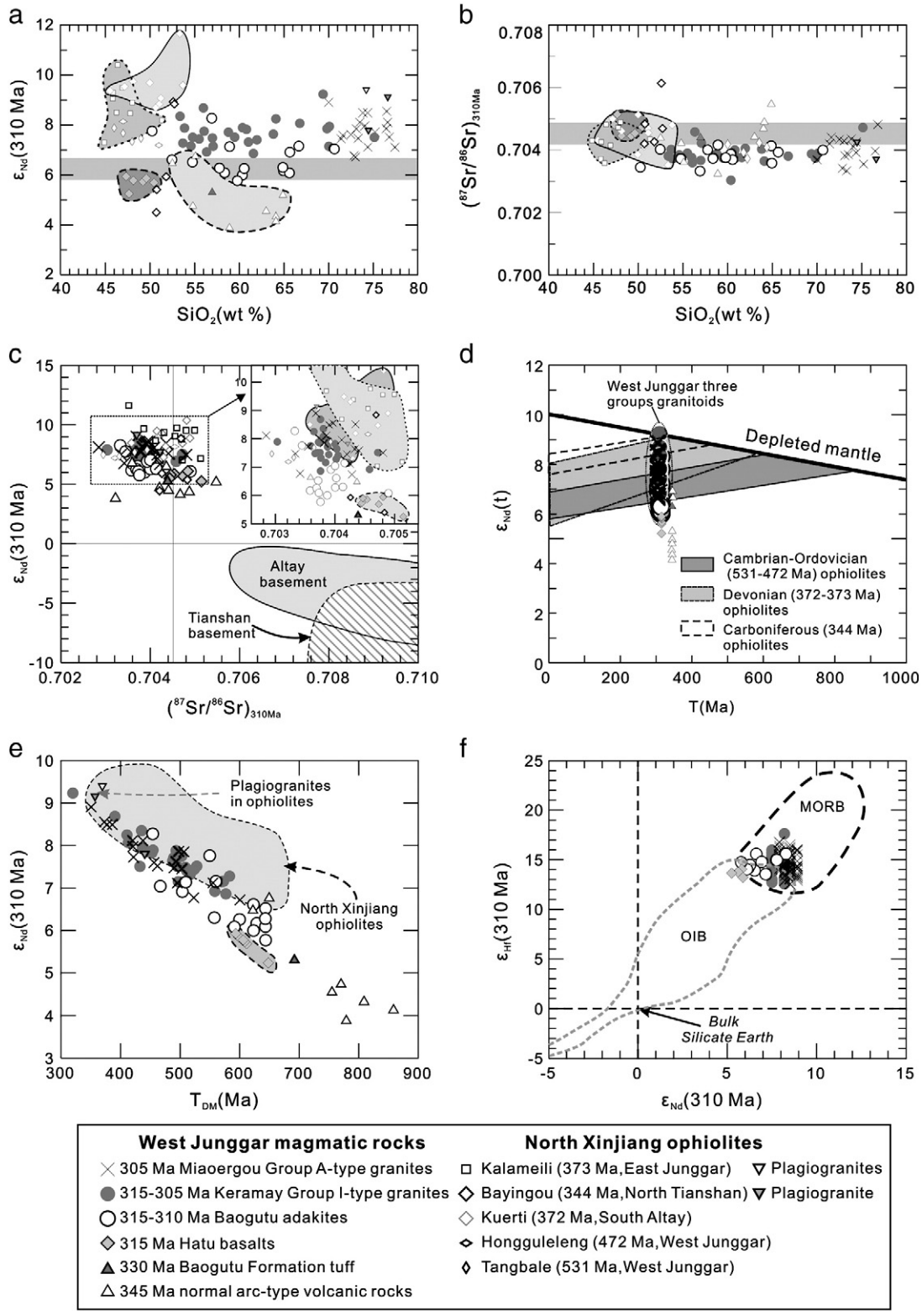

Fig. 4. Plots of (a) $\varepsilon_{Nd}(t)$ values versus SiO_2 and (b–d) Sr–Nd–Hf isotopic ratios and Nd model ages of the Miaoergou Group A-type granites, the Keramay Group I-type granites and the Baogutu adakties compared to North Xinjiang ophiolites and Carboniferous basalts in the western Junggar region. The 315 Ma Hatu basalts are from Tang et al. (submitted for publication); the 330 Ma Baogutu Formation tuff is from Shen et al. (2009); and the 345 Ma normal arc-type volcanic rocks are from Geng et al. (2011). The data for North Xinjiang ophiolites are from Table 4. The data for the Altay and Tianshan basements are from Hu et al. (2000). Other data sources are the same as for Fig. 3.

5.2. Contribution of recycled oceanic crust to continental crustal growth

Irrespective of the various crustal growth models applied to the CAOB, there is increasing evidence for the existence and subduction of a Carboniferous ocean basin and a Carboniferous intra-oceanic arc in the western Junggar region (Geng et al., 2009; Tang et al., 2010; Xiao et al., 2008; Zhang et al., 2011). Based on such evidence, a ridge subduction and slab edge partial melting model (Fig. 5) has been proposed to account for the western Junggar Late Carboniferous granitoids (Geng et al., 2009; Tang et al., 2010; Zhang et al., 2011).

Table 4
Sr–Nd isotope compositions of the Pre-Permian ophiolites from around Junggar Basin.

Ophiolites	Age (Ma)	Sample	SiO_2	Sm	Nd	Rb	Sr	$(^{87}Sr/^{86}Sr)_s$	$(^{143}Nd/^{144}Nd)_s$	$(^{87}Rb/^{86}Sr)s$	$(^{147}Sm/^{144}Nd)s$	$(^{87}Sr/^{86}Sr)_i$	εNd(t)	T_{1DM}	T_{2DM}	Refs
Kelameili	373	KL-01	49.96	3.36	10.5	3.03	615	0.703917	0.513132	0.014	0.196	0.703856	9.7	160	283	1
Kelameili	373	KL-12	47.14	0.99	2.53	0.08	225	0.705	0.513212	0.001	0.238	0.704996	9.6	379	294	1
Kelameili	373	KL-14	38.47	1.73	6.62	10.9	192	0.705417	0.512922	0.16	0.159	0.704709	7	641	502	1
Kelameili	373	KL-21	50.66	2.13	7.76	10.8	913	0.704265	0.513023	0.034	0.245	0.704117	8.7	420	366	1
Kelameili	373	KL-24	45.5	2.18	6.27	0.25	67	0.704356	0.513149	0.011	0.212	0.704309	9.4	154	309	1
Kelameili	373	KL-27	50	1.5	4.39	3.32	131	0.705443	0.513029	0.071	0.208	0.705128	7.2	3272	489	1
Kelameili	373	03T-10-3	51.03	2.4	8.21	3.7	210	0.704918	0.513052	0.05	0.28	0.704699	8.8	424	355	2
Kelameili	373	03T-10-4	51.2	2.91	7.96	2.5	185	0.704722	0.513155	0.038	0.223	0.704554	9.1	69	335	2
Kelameili	373	03T-11	48.12	2.49	6.86	3	267	0.704736	0.513187	0.032	0.221	0.704596	9.8	750	278	2
Kelameili	373	03T-6	53.34	1.79	5.51	14	156	0.704636	0.513237	0.253	0.198	0.703519	11.7			2
Kelameili	373	03T-9	53.8	2.74	8.06	3.5	194	0.705026	0.513148	0.051	0.207	0.704802	9.6	68	295	2
Kelameili	373	SJ24[a]	74.47	2.99	8.95				0.513133		0. 2017		9.41	260	306	3
Kuerti	372	X-26-2	46.24	4.53	14.6	1.02	259	0.70358	0.513054	0.011	0.189	0.70358	8.5	598	387	4
Kuerti	372	X-27-4	44.87	3.22	9.17	10.1	294	0.7043	0.513053	0.097	0.214	0.7043	7.3		470	4
Kuerti	373	X-27-5	47.78	3.3	9.49	7.02	246	0.70472	0.513108	0.08	0.212	0.70472	8.5	3321	375	4
Kuerti	372	X-27-8	51.33	4.44	13.1	0.45	48	0.704346	0.513084	0.026	0.206	0.704346	8.2	1394	396	4
Kuerti	372	X-35-1	46.41	3.57	1.79	2.98	161	0.704817	0.513436	0.052	0.305	0.704817	10.4	476	152	4
Kuerti	372	K-33	45.87	2.19	6.06	6.05	154	0.70426	0.51316	0.111	0.22	0.70426	9.3	217	318	5
Kuerti	372	K-36-4	48.02	3.09	9.18	6.5	188	0.70489	0.51311	0.097	0.205	0.70489	8.9	713	349	5
Kuerti	372	K-32	45.83	5.63	22	2.99	155	0.70371	0.513	0.054	0.156	0.70371	9.1	398	366	5
Kuerti	372	K-34-4	46.9	4.47	14.7	4.79	171	0.70415	0.51309	0.079	0.185	0.70415	9.5	323	316	5
Bayingou	344	011B77[a]	76.62	0.5	1.7	5	197	0.704011	0.51307	0.072	0.179	0.703695	9.1	358	329	6
Bayingou	344	011BT8[a]	74.45	0.54	1.6	5.9	211	0.704564	0.513055	0.079	0.205	0.704216	7.8	1782	439	6
Bayingou	344	011B78	52.72	1.7	5	13.3	67	0.70716	0.513112	0.56	0.207	0.70469	8.8	903	354	6
Bayingou	344	011B79	51.8	1.8	6	15.7	127	0.705799	0.512913	0.349	0.183	0.704261	5.9	1169	593	6
Bayingou	344	011B71	50.76	2	6	8.3	160	0.705476	0.512927	0.146	0.203	0.704831	5.4	3161	636	6
Bayingou	344	011B75	52.6	3.1	10.7	0.6	127	0.706195	0.513054	0.013	0.176	0.706136	8.9	397	346	6
Bayingou	344	011B58	50.7	2.3	6.3	6.1	117	0.704848	0.51292	0.147	0.222	0.704199	4.5		711	6
Hongguleleng	472	H-5-2		3.641	24.31	12.25	332.6	0.70344	0.51287	0.03682	0.1495	0.703192	7.4	608	669	7
Hongguleleng	472	H-5-5		3.152	16.05	6.933	302.1	0.7047	0.51306	0.02295	0.1964	0.704546	8.3	536	807	7
Tangbale	488	TB-37		3.123	23.11	67.07	297.8	0.70553	0.51284	0.2252	0.1351	0.703964	7.8	587	605	7
Tangbale	488	TB-76		2.482	17.94	47.52	245.4	0.70462	0.51284	0.1352	0.1384	0.703680	7.6	604	631	7
Tangbale	488	T-4-1		3.603	17.54	70.82	136.1	0.70702	0.51304	0.5205	0.2054	0.703401	7.3	627	2056	7
Tangbale	488	T-6-1		2.869	18.82	53.24	146.1	0.70555	0.51288	0.3644	0.1524	0.703016	7.5	612	676	7
Aermantai	503	XJ-2		1.481	8.247	59.71	1150	0.70457	0.51288	0.0519	0.1798	0.704198	5.8	762	1221	8
Aermantai	503	XJ-3		1.912	12.06	152	106.7	0.7055	0.51282	0.2217	0.1586	0.703911	6.0	746	917	8
Aermantai	503	XJ-6		1.916	11.43	86.69	552.1	0.70549	0.51287	0.157	0.1676	0.704365	6.4	714	931	8
Aermantai	503	XJ-8		3	18.46	134.4	455	0.7059	0.51284	0.2953	0.1625	0.703783	6.1	735	928	8
Aermantai	503	XJ-14		4.306	36.23	20.48	380.1	0.70468	0.51267	0.05387	0.1189	0.704294	5.6	777	775	8
Aermantai	503	XJ-17		2.451	16.74	46.1	235.4	0.70554	0.51277	0.1959	0.1464	0.704136	5.8	762	864	8
Aermantai	503	XJ-19		3.938	27.02	44.07	270.2	0.70547	0.51276	0.1631	0.1458	0.704301	5.7	775	879	8
Aermantai	503	XJ-20		4.387	30.21	5.327	638.5	0.70411	0.51277	0.00834	0.1452	0.704050	5.9	756	849	8

Data sources: 1—Ma (2007); 2—Liu et al. (2007); 3—Tang et al. (2007); 4—Xu et al. (2003); 5—Ma et al. (2009); 6—Xu et al. (2006); 7—Zhang and Huang (1992); 8—Huang et al. (1997).

[a] Plagiogranite. Other samples are basalts or gabbros.

Given that the Miaoergou Group A-type granites and Keramy Group I-type granitoids have more depleted Nd–Sr–Hf isotope compositions than those of coeval basalts in the same area, they could not have been generated by partial melting of juvenile lower crust (Geng et al., 2009) or by processes involving mantle-derived magmas (e.g., magma mixing or assimilation and fractional crystallization (AFC) processes involving mantle-derived magmas) as suggested by Chen and Arakawa (2005). Although their isotopic compositions and intermediate-felsic composition suggest that they were derived from oceanic crust, they are distinct from the Baogutu adakites in that they have moderate to pronounced negative Eu anomalies, relatively low Sr and Sr/Y ratios and are unlikely to have been derived from actively subducting oceanic crust (Fig. 3a; Table 4).

It was possible, however, that the A-type and I-type granitoids were generated by partial melting of oceanic crust stored in the middle and (or) lower crust. The middle–lower crust of the western Junggar intra-oceanic arc probably consisted of underthrust or trapped oceanic crust (White et al., 2003; Zagorevski et al., 2009), or the arc itself was built upon oceanic crust (Sengör et al., 1993). Relatively high concentrations of heavy REE and strongly negative Eu anomalies indicate that the Miaoergou Group A-type granites were likely derived from an oceanic crustal source buried within the stability field of plagioclase. The weakly negative Eu anomalies of the Keramay Group I-type granitoids suggest melting of a lower crustal source at relative high pressures with high amphibole concentration and minor plagioclase in the residue. On the Sr/Y vs. Y diagram (Fig. 3e), the Baogutu adakites have distinctly higher Sr/Y ratios and lower Y contents than the Keramay I-type granitoids, indicating melting of subducted oceanic crust at greater depths and a garnet amphibolite residuum for the adakite melts (Moyen, 2009). The heat source for melting was likely the upwelling asthenospheric mantle through a slab window in a ridge subduction setting (Fig. 5).

The petrogenesis of the three groups of granitoids (adakites, I and A type granitoids) in the western Junggar region thus provides a strong case for the production of juvenile continental crust from recycled oceanic crust including partial melting of subducted oceanic crust and oceanic crust residing in the mid-lower crust.

Establishing a relationship between continental crustal growth and near-contemporaneous oceanic crustal recycling in the western Junggar region has important implications for the development of the CAOB, and for the formation and evolution of the continental crust in general (e.g., Windley et al., 2007). This study demonstrates

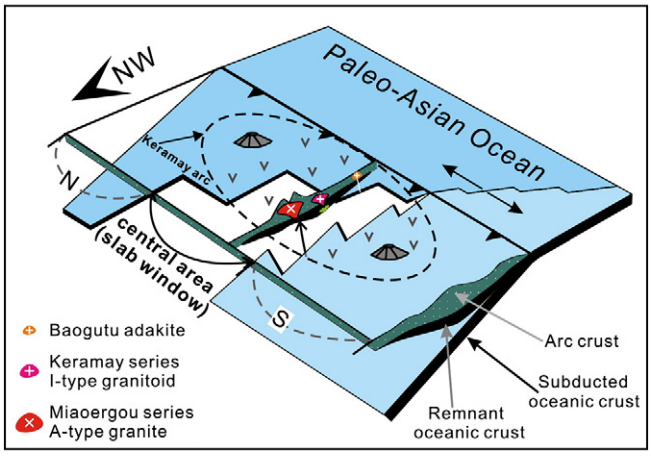

Fig. 5. A formation model of the Miaoergou Group A-type granites, the Keramay Group I-type granites and the Baogutu adakites in the western Junggar region during the Late Carboniferous. These adakites were derived from recycled oceanic crust by melting of subducted oceanic crust (Tang et al., 2010), and the I and A-type granites were mainly generated by melting of intra-oceanic arc middle–lower crust mainly consisting of oceanic crust. N — northern area; S — southern area.

that, irrespective of evolving mantle thermal conditions since the Archean, the ridge subduction–slab window setting has the capacity to create significant volumes of juvenile continental crust where appropriate basaltic sources are available in the middle–lower crust of intra-oceanic arcs (Fig. 5) and active continental margins. Our results, based on a particularly favorable range of isotopic compositions among the components (or possible components) involved, demonstrate that recycling of oceanic lithosphere has continued to play a crucial role in the evolution and growth of the Earth's continental crust since the Archean. Although processes such as partial melting of underplated basaltic lower crust, subduction erosion and lower crustal delamination have also made important contributions (e.g., Atherton and Petford, 1993; Clift and Vannucchi, 2004; Clift et al., 2009; Jahn et al., 2000; Rudnick, 1995), it is likely that, in many instances, the recycling of oceanic lithosphere has been overlooked because of a lack of distinctive isotopic criteria.

Supplementary materials related to this article can be found online at doi:10.1016/j.lithos.2011.11.003.

Acknowledgments

We sincerely thank Professors Nelson Eby and Robert Kerrich, and an anonymous reviewer for their constructive and helpful reviews on this manuscript. We appreciate the assistance of Drs. Jinhui Yang, Xirong Liang, Xianglin Tu and Yueheng Yang and Mrs. Ying Liu for the zircon age and geochemical analysis. This study was jointly supported by the Major State Basic Research Program (973 Program) of People's Republic of China (No. 2007CB411308 and 2010CB808906), and the National Natural Science Foundation of China (Grants Nos. 41025006 and 41073029). This is a contribution No. IS-1412 from GIG-CAS and TIGeR publication #392.

References

An, F., Zhu, Y.F., 2009. SHRIMP U–Pb zircon ages of the tuff in Baogutu Formation and their geological significances. Acta Petrologica Sinica 25, 1437–1445 (in Chinese with English abstract).
Atherton, M.P., Petford, N., 1993. Generation of sodium-rich magmas from newly underplated basaltic crust. Nature 362, 144–146.
Belousova, E.A., Kostitsyn, Y.A., Griffin, W.L., Begg, G.C., O'Reilly, S.Y., Pearson, N.J., 2010. The growth of the continental crust: constraints from zircon Hf-isotope data. Lithos 119, 457–466.
Clift, P., Vannucchi, P., 2004. Controls on tectonic accretion versus erosion in subduction zones: Implications for the origin and recycling of the continental crust. Reviews of Geophysics 42, RG2001. doi:10.1029/2003RG000127.
Clift, P.D., Vannucchi, P., Morgan, J.P., 2009. Crustal redistribution, crust–mantle recycling and Phanerozoic evolution of the continental crust. Earth-Science Reviews 97, 80–104.
Chappell, B.W., White, A.J.R., 1992. I- and S-type granites in the Lachlan Fold Belt. Transactions of the Royal Society of Edinburgh: Earth Sciences 83, 1–26.
Chen, B., Arakawa, Y., 2005. Elemental and Nd–Sr isotopic geochemistry of granitoids from the West Junggar foldbelt (NW China), with implications for Phanerozoic continental growth. Geochimica et Cosmochimica Acta 69, 1307–1320.
Chen, B., Jahn, B.M., 2004. Genesis of post-collisional granitoids and basement nature of the Junggar Terrane, NW China: Nd–Sr isotope and trace element evidence. Journal of Asian Earth Sciences 23, 691–703.
Collins, W.J., Belousova, E.A., Kemp, A.I.S., Murphy, J.B., 2011. Two contrasting Phanerozoic orogenic systems revealed by hafnium isotope data. Nature Geoscience 4, 333–337.
Condie, K.C., 2000. Episodic continental growth models: afterthoughts and extensions. Tectonophysics 322, 153–162.
Defant, M.J., Drummond, M.S., 1993. Mount St. Helens: potential example of the partial melting of the subducted lithosphere in a volcanic arc. Geology 21, 547–550.
Drummond, M.S., Defant, M.J., 1990. A model for trondhjemite–tonalite–dacite genesis and crustal growth via slab melting: Archaean to modern comparisons. Journal of Geophysical Research 95, 21503–21521.
Eby, G.N., 1990. The A-type granitoids: a review of their occurrence and chemical characteristics and speculations on their petrogenesis. Lithos 26, 115–134.
Eby, G.N., 1992. Chemical subdivision of the A-type granitoids: petrogenetic and tectonic implications. Geology 20, 641–644.
Gao, S., Liu, X.-M., Yuan, H.-L., Hattendorf, B., Günther, D., Chen, L., Hu, S.-H., 2002. Determination of forty two major and trace elements in USGS and NIST SRM glasses by laser ablation inductively coupled plasma–mass spectrometry. Geostandards and Geoanalytical Research 26, 181–195.
Geng, H.Y., Sun, M., Yuan, C., Xiao, W., Xian, W., Zhao, G., Zhang, L., Wong, K., Wu, F., 2009. Geochemical, Sr–Nd and zircon U–Pb–Hf isotopic studies of Late Carboniferous magmatism in the West Junggar, Xinjiang: implications for ridge subduction? Chemical Geology 266, 364–389.
Geng, H.Y., Sun, M., Yuan, C., Zhao, G.C., Xiao, W.J., 2011. Geochemical and geochronological study of early Carboniferous volcanic rocks from the West Junggar: petrogeneses and tectonic implications. Journal of Asian Earth Sciences. doi:10.1016/j.jseaes.2011.1001.1006.
Han, B.F., Ji, J.Q., Song, B., Chen, L.H., Zhang, L., 2006. Late Paleozoic vertical growth of continental crust around the Junggar Basin, Xinjiang, China (Part I). Timing of post-collisional plutonism. Acta Petrologica Sinica 22, 1077–1086 (in Chinese with English abstract).
Hawkesworth, C.J., Dhuime, B., Pietranik, A.B., Cawood, P.A., Kemp, A.I.S., Storey, C.D., 2010. The generation and evolution of the continental crust. Journal of the Geological Society 167, 229–248.
Hu, A.Q., Jahn, B.M., Zhang, G.X., Chen, Y.B., Zhang, Q.F., 2000. Crustal evolution and Phanerozoic crustal growth in northern Xinjiang: Nd isotopic evidence. Part I. Isotopic characterization of basement rocks. Tectonophysics 328, 15–51.
Huang, X., Jin, C.W., Sun, B.S., Jun, P., Zhang, R.H., 1997. Study on the age of Aermantai ophiolite, Xinjiang by Nd–Sr isotope geology. Acta Petrologica Sinica 13, 85–91 (in Chinese with English abstract).
Jackson, S.E., Pearson, N.J., Belousova, E., Griffin, W.L., 2004. The application of laser ablation-inductively coupled plasma–mass spectrometry (LA-ICP–MS) to in situ U–Pb geochronology. Chemical Geology 211, 47–69.
Jahn, B.M., 2004. The Central Asian Orogenic Belt and growth of the continental crust in the Phanerozoic. In: Malpas, J., Fletcher, C.J.N., Ali, J.R., Aichison, J.C. (Eds.), Aspects of the Tectonic Evolution of China. Geological Society London, Special Publications, London, pp. 73–100.
Jahn, B.M., Wu, F.Y., Chen, B., 2000. Massive granitoid generation in Central Asia: Nd isotope evidence and implication for continental growth in the Phanerozoic. Episodes 23, 82–92.
Kemp, A.I.S., Hawkesworth, C.J., 2003. Granitic perspectives on the generation and secular evolution of the continental crust. The Crust. : Treatise on Geochemistry, 3. Elsevier, Amsterdam, Netherlands, pp. 349–410.
King, P.L., White, A.J.R., Chappell, B.W., Allen, C.M., 1997. Characterization and origin of aluminous A-type granites from the Lachlan Fold Belt, Southeastern Australia. Journal of petrology 38, 371–391.
Kröner, A., Windley, B.F., Badarch, G., Tomurtogoo, O., Hegner, E., Jahn, B.M., Gruschka, S., Khain, E.V., Demoux, A., Wingate, M.T.D., 2007. Accretionary growth and crust formation in the Central Asian Orogenic Belt and comparison with the Arabian–Nubian shield. In: Hatcher Jr., R.D., Carlson, M.P., McBride, J.H. (Eds.), A 4-D framework of continental crust, Volume 200, Geological Society of America Memoirs, pp. 181–209.
Konopelko, D., Biske, G., Seltmann, R., Eklund, O., Belyatsky, B., 2007. Hercynian post-collisional A-type granites of the Kokshaal Range, Southern Tien Shan, Kyrgyzstan. Lithos 97, 140–160.
Li, X.H., Li, Z.X., Wingate, M.T.D., Chung, S.L., Liu, Y., Lin, G.C., Li, W.X., 2006. Geochemistry of the 755 Ma Mundine Well dyke swarm, northwestern Australia: part of a Neoproterozoic mantle superplume beneath Rodinia? Precambrian Research 146 (1–2), 1–15.
Li, X.H., Li, Z.X., Zhou, H., Liu, Y., Kinny, P.D., 2002. U–Pb zircon geochronology, geochemistry and Nd isotopic study of Neoproterozoic bimodal volcanic rocks in the Kangdian Rift of South China: implications for the initial rifting of Rodinia. Precambrian Research 113 (1–2), 135–154.
Liu, W., Pan, X.F., Liu, D.Y., Chen, Z.Y., 2009. Three-step continental-crust growth from subduction accretion and underplating, through intermediary differentiation, to granitoid production. Journal of Earth Sciences 98, 1413–1439.
Liu, W., Siebel, W., Li, X.J., Pan, X.F., 2005. Petrogenesis of the Linxi granitoids, northern Inner Mongolia of China: constraints on basaltic underplating. Chemical Geology 219, 5–35.

Liu, X.J., Xu, J.F., Hou, Q.Y., Bai, Z.H., Lei, M., 2007. Geochemical characteristics of Karamaili ophiolite in east Junggar, Xingjiang : products of ridge subduction. Acta Petrologica Sinica 23, 1591–1602 (in Chinese with English abstract).
Liu, Y.S., Gao, S., Gao, C.G., Wang, D.B., Zong, K.Q., Hu, Z.C., 2010. Timing of melt–peridotite interactions in xenoliths of the Trans-North China Orogen: U–Pb dating, Hf isotopes and trace elements in zircon. Journal of Petrology 51 (1–2), 537–571.
Ludwig, K.R., 2003. User's manual for Isoplot 3.00: a geochronological toolkit for Microsoft Excel. Berkeley Geochronology Center Special Publication 4, 1–70.
Ma, L., Zhang, H.X., Zhang, B.Y., Niu, H.C., 2009. Protoliths reconstruction of amphiolites from Kuerti ophiolites in north Xinjiang and its petrogenesis. Acta Petrologica Sinica 24 (4), 673–680 (in Chinese with English abstract).
Ma, Z.P., 2007. Study on the Ophiolite from Tianshan and Adjacent Areas and its Relation with the Evolution of the Paleozoic Oceans. Northwestern University, Xi'an, p. 129 (in Chinese with English abstract).
Martin, H., Smithies, R.H., Rapp, R., Moyen, J.F., Champion, D., 2005. An overview of adakite, tonalite–trondhjemite–granodiorite (TTG), and sanukitoid: relationships and some implications for crustal evolution. Lithos 79, 1–24.
Mints, M.V., Belousova, E.A., Konilov, A.N., Natapov, L.M., Shchipansky, A.A., Griffin, W.L., O'Reilly, S.Y., Dokukina, K.A., Kaulina, T.V., 2010. Mesoarchean subduction processes: 2.87 Ga eclogites from the Kola Peninsula, Russia. Geology 38, 739–742.
Moyen, J.F., 2009. High Sr/Y and La/Yb ratios: the meaning of the "adakitic signature". Lithos 112, 556–574.
Peacock, S.M., Rushmer, T., Thompson, A.B., 1994. Partial melting of subducting oceanic-crust. Earth and Planetary Science Letters 121, 227–244.
Rudnick, R.L., 1995. Making continental crust. Nature 378, 573–578.
Sengör, A.M.C., Natal'in, B.A., Burtman, V.S., 1993. Evolution of the Altaid tectonic collage and Palaeozoic crustal growth in Eurasia. Nature 364, 299–307.
Shen, P., Shen, Y., Liu, T., Meng, L., Dai, H., Yang, Y., 2009. Geochemical signature of porphyries in the Baogutu porphyry copper belt, western Junggar, NW China. Gondwana Research 16, 227–242.
Stein, M., Hofmann, A.W., 1994. Mantle plumes and episodic crustal growth. Nature 372, 63–68.
Tang, G.J., Wang, Q., Wyman, D.A., Li, Z.X., Zhao, Z.H., Jia, X.H., Jiang, Z.Q., 2010. Ridge subduction and crustal growth in the Central Asian Orogenic Belt: evidence from Late Carboniferous adakites and high-Mg diorites in the western Junggar region, northern Xinjiang (west China). Chemical Geology 227, 281–300.
Tang, G.J., Wyman, D.A., Wang, Q., Li, Z.X., Zhao, Z.H., Sun, W.D., Li, J., (submitted to publication). Asthenosphere–lithosphere interaction triggered by a slab window during ridge subduction: Trace element and Sr–Nd–Hf–Os isotopic evidence from Late Carboniferous tholeiites in the western Junggar area (NW China) Earth and Planetary Science Letters.
Tang, G.J., 2011. Petrogenesis of Late Paleozoic magmatic rocks in the western Tianshan and western Junggar regions (north Xinjiang): implications for crustal growth and Cu–Au mineralization. Ph. D. thesis, Chinese Academy of Sciences, Beijing, China (in Chinese with English abstract). P. 1–251.
Tang, H.F., Su, Y.P., Liu, C.Q., Hou, G.S., Wang, Y.B., 2007. Zircon U–Pb age of the plagiogranite in Kalamaili belet, Northern Xinjiang and its tectonic implications. Geotectonica et Metallogenia 31, 110–117 (in Chinese with English abstract).
Whalen, J.B., Currie, K.L., Chappell, B.W., 1987. A-type granites: geochemical characteristics, discrimination and petrogenesis. Contributions to Mineralogy and Petrology 95, 407–419.
White, D.J., Musacchio, G., Helmstaedt, H.H., Harrap, R.M., Thurston, P.C., van der Velden, A., Hall, K., 2003. Images of a lower-crustal oceanic slab: Direct evidence for tectonic accretion in the Archean western Superior province. Geology 31, 997–1000.
Windley, B.F., Alexeiev, D., Xiao, W., Kroner, A., Badarch, G., 2007. Tectonic models for accretion of the Central Asian Orogenic Belt. Journal of the Geological Society 164, 31–47.
Wu, F.Y., Jahn, B.M., Wilde, S., Sun, D.Y., 2000. Phanerozoic crustal growth: U–Pb and Sr–Nd isotopic evidence from the granites in northeastern China. Tectonophysics 328, 89–113.
Wu, F.Y., Yang, Y.H., Xie, L.W., Yang, J.H., Xu, P., 2006. Hf isotopic compositions of the standard zircons and baddeleyites used in U–Pb geochronology. Chemical Geology 234, 105–126.
Xiao, W.J., Windley, B.F., Badarch, G., Sun, S., Li, J., Qin, K., Wang, Z., 2004. Palaeozoic accretionary and convergent tectonics of the southern Altaids: implications for the growth of Central Asia. Journal of the Geological Society 161, 339–342.
Xiao, W.J., Han, C.M., Yuan, C., Sun, M., Lin, S.F., Chen, H.L., Li, Z.L., Li, J.L., Sun, S., 2008. Middle Cambrian to Permian subduction-related accretionary orogenesis of Northern Xinjiang, NW China. Implications for the tectonic evolution of central Asia. Journal of Asian Earth Sciences 32, 102–117.
Xiao, W.J., Windley, B.F., Yuan, C., Sun, M., Han, C.M., Lin, S.F., Chen, H.L., Yan, Q.R., Liu, D.Y., Qin, K.Z., Li, J.L., Sun, S., 2009. Paleozoic multiple subduction–accretion processes of the southern Altaids. American Journal of Science 309, 221–270.
Xu, J.F., Castillo, P.R., Chen, F.R., Niu, H.C., Yu, X.Y., Zhen, Z.P., 2003. Geochemistry of late Paleozoic mafic igneous rocks from the Kuerti area, Xinjiang, northwest China: implications for backarc mantle evolution. Chemical Geology 193, 137–154.
Xu, X.Y., Xia, L.Q., Ma, Z.P., Wang, Y.B., Xia, Z.C., Li, X.M., Wang, L.S., 2006. SHRIMP zircon U–Pb geochronology of the plagiogranites from Bayringou ophiolite in North Tianshan Mountains and the petrogenesis of the ophiolite. Acta Petrologica Sinica 22, 83–94 (in Chinese with English abstract).
Zagorevski, A., van Lissenberg, C.J., Staal, C.R., 2009. Dynamics of accretion of arc and back-arc crust to continental margins; inferences from the Annieopsquotch accretionary tract, Newfoundland Appalachians. Tectonophysics 479, 150–164.
Zhang, C., Huang, X., 1992. Age and tectonic settings of ophiolites in west Junggar, Xinjiang. Geology Review 38, 509–524 (in Chinese with English abstract).
Zhang, C.L., Li, Z.X., Li, X.H., Xu, Y.G., Zhou, G., Ye, H.M., 2010. A Permian large igneous province in Tarim and Central Asian Orogenic Belt (CAOB), NW China: results of a ca. 275 Ma mantle plume? Geological Society of America Bulletin 122, 2020–2040.
Zhang, J.E., Xiao, W.J., Han, C.M., Mao, Q.G., Ao, S.J., Guo, Q.Q., Ma, C., 2011. A Devonian to Carboniferous intra-oceanic subduction system in Western Junggar, NW China. Lithos. doi:10.1016/j.lithos.2011.03.013.
Zheng, J.P., Sun, M., Zhao, G.C., Robinson, P.T., Wang, F.Z., 2007. Elemental and Sr–Nd–Pb isotopic geochemistry of Late Paleozoic volcanic rocks beneath the Junggar basin, NW China: implications for the formation and evolution of the basin basement. Journal of Asian Earth Sciences 29, 778–794.
Zhou, M.F., Zhao, J.H., Jiang, C.Y., Gao, J.F., Wang, W., Yang, S.H., 2009. OIB-like, heterogeneous mantle sources of Permian basaltic magmatism in the western Tarim Basin, NW China: Implications for a possible Permian large igneous province. Lithos 113, 583–594.
Zhou, M.F., Michael Lesher, C., Yang, Z.G., Li, J.W., Sun, M., 2004. Geochemistry and petrogenesis of 270 Ma Ni–Cu–(PGE) sulfide-bearing mafic intrusions in the Huangshan district, Eastern Xinjiang, Northwest China: implications for the tectonic evolution of the Central Asian orogenic belt. Chemical Geology 209, 233–257.